Impact of Optical Nonlinearity on Performance of Photonic Time-Stretch Analog-to-Digital Converter

Ali M. Fard, *Student Member, IEEE*, Peter T. S. DeVore, Daniel R. Solli, and Bahram Jalali, *Fellow, IEEE*

***Abstract*—Wideband real-time analog-to-digital converters are the central tools in waveform analyzers, communication systems, and radar technology. Photonic time-stretch analog-to-digital converters (TSADCs) utilize a broadband optical source and an optical link to extend the capabilities of real-time digitizers, allowing acquisition of wideband radio frequency (RF) signals with high resolution. In the TSADC, it is desirable to improve the signal-to-noise-and-distortion ratio and effective number of bits by increasing the optical power. Here, we numerically evaluate the impact of optical nonlinearity on TSADC performance. It is demonstrated that the optical nonlinearity can impose an upper limit on the effective number of bits and that the RF bandwidth limitation due to dispersion penalty depends on optical power. The trends presented here can also be applied to other optical links in which optical nonlinearity and dispersion are significant.**

***Index Terms*—Microwave photonics, optical Kerr nonlinearity, fiber nonlinear optics, analog-to-digital conversion, optical signal processing, optical fiber communication.**

I. Introduction

ANALOG-TO-DIGITAL CONVERTERS (ADCs) play a crucial role in one's ability to harness the power of digital signal processing (DSP). The demand for high-resolution, high-bandwidth ADCs is growing very rapidly in many extremely important applications, such as advanced laboratory instruments, military systems, biomedical imaging, and industrial applications. In military applications, such ADCs are integral components in radar systems, receivers, and battlefield airborne communications nodes [1]. In biomedical and other critical sensing applications such as flow cytometry, fast digitzers are the enabling technology for high-throughput analysis [2], [3]. Moreover, the rapid growth of internet traffic requires optical networks with high capacity [4]–[8]. Such networks employing advanced data modulation formats [6] rely on high-bandwidth real-time digitizers to receive and digitally equalize the high-speed data streams.

The photonic time-stretch analog-to-digital converter (TSADC) [9]–[11] can provide continuous digitization of ultrahigh-bandwidth electrical signals with high resolution, which cannot be achieved by purely electronic ADCs [12]. The TSADC stretches the radio frequency (RF) signal in time by employing a chirped broadband optical source and a dispersive analog optical link as illustrated in Fig. 1. The chirped broadband optical source consists of a mode-locked laser followed by a dispersive medium. The RF signal to be captured is modulated on the chirped optical pulses using an intensity modulator (e.g., Mach–Zehnder modulator) and group-velocity dispersion (GVD) is then exploited to stretch the intensity-modulated optical pulses in time. Dispersion compensating fiber (DCF) provides a large dispersion-to-loss ratio with minimal phase distortion over a wide optical bandwidth and is ideal for pre-chirping and time-stretching in the TSADC (Fig. 1). Under various circumstances, it may be desirable to increase the optical power to improve the performance of TSADC. For example, one may wish to increase the power when attempting to improve the signal-to-noise ratio. In addition, for continuous-time operation, the TSADC uses multiple parallel wavelength channels and digitizers to time-interleave the time-stretched segments of the RF signal [11], [13]; when multiple wavelength channels are employed, intensity-modulated optical pulses with high peak power are required. However, when high-power pulses propagate inside the dispersive fiber, both optical nonlinearity and dispersion influence the shape and spectrum of the pulses. This leads to amplitude distortions and can degrade the signal-to-noise-and-distortion ratio (SNDR) and the effective number of bits (ENOB) under certain conditions.

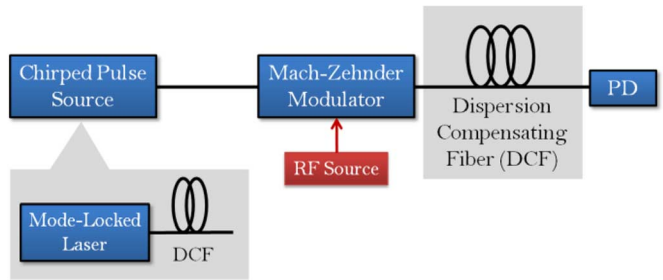

Fig. 1. Block diagram of the photonic time-stretch analog-to-digital converter (TSADC). The chirped pulse source consists of a mode-locked laser followed by a dispersive medium. PD: Photodetector, RF: radio frequency.

In this paper, we report the impact of optical Kerr nonlinearity on the performance of the TSADC. The nonlinear interaction of the optical field inside the fiber used for time-stretch is numerically simulated using the split-step Fourier method [14]. We show that nonlinear degradation of the RF signal (measured by the carrier-to-interference ratio) is greater when smaller optical bandwidths are employed; increasing the optical bandwidth improves system performance. It is also shown that nonlinearity

Manuscript received March 02, 2011; revised May 05, 2011; accepted May 10, 2011. Date of publication May 23, 2011; date of current version June 15, 2011. This work was supported by US Defense Advanced Research Projects Agency under RADER program.

The authors are with Photonics Laboratory, Department of Electrical Engineering, University of California Los Angeles, Los Angeles, CA 90095 USA (email: motafakk@ee.ucla.edu).

Digital Object Identifier 10.1109/JLT.2011.2157304

tends to reduce the RF bandwidth of the system (due to the frequency-fading phenomenon known as dispersion penalty [11]) as the optical power is increased. The rest of this paper is structured as follows. Section II discusses optical nonlinearity in the context of TSADC and presents an analytical model that provides qualitative insight into the numerical results presented in the subsequent section. The impact of nonlinearity on the RF signal including the carrier-to-interference ratio and dispersion penalty are shown in Section III.

II. Optical Fiber Nonlinearity in Photonic Time-Stretch Analog-to-Digital Converter

In order to operate multiple wavelength channels, it is desirable to utilize high optical power in the TSADC system; increased power facilitates higher SNDR and, hence, higher ENOB. However, high intensity causes the pulse propagation to deviate from the linear regime. Therefore, it is imperative to consider the effect of fiber nonlinearity (Kerr effect) on the performance of the TSADC. The basic equation that governs the propagation of optical pulses in the presence of disperison and optical nonlinearity is the nonlinear Schrödinger equation (NLSE)

$$\frac{\partial A}{\partial z}+\frac{i\beta_2}{2}\frac{\partial^2 A}{\partial t^2}=-\frac{\alpha}{2}A+i\gamma|A|^2A \tag{1}$$

where α is the attenuation constant, β_2 is the GVD parameter (the second derivative with respect to angular frequency of the modal wave number), γ is the nonlinear coefficient related to the nonlinear index n_2 by $\gamma=(n_2\omega_0)/(cA_{\text{eff}})$, and A_{eff} is the effective mode area of the fiber [14]. A in (1) is the slowly varying envelope proportional to the optical field. Equation (1) has been successful in explaining a large number of nonlinear effects, e.g., self-phase modulation and four-wave mixing, which are the main causes of nonlinear optical distortions in the TSADC. The split-step Fourier method is commonly employed to solve the NLSE numerically, obtaining an approximate solution by assuming that the dispersive and nonlinear effects act independently over a very small length of fiber [14]. We also found that the local-error method algorithm [15] reduces the computation time for split-step calculations, and offers a significant improvement in the context of TSADC, where a broad time window and fine time resolution are needed. Here we consider the impact of optical nonlinearity in the second dispersive fiber (i.e., dispersive fiber after the intensity modulator) because it is in this step that the nonlinearity affects the RF signal. In order to significantly reduce the number of sample points and simulation run-time, we only evaluate a single broadband optical pulse propagating through the TSADC in each simulation.

In an effort to explain the effect of optical nonlinearity, we first introduce an analytical model for the optical envelope without modulation, which helps to qualitatively explain the results shown in the next section. We begin with an unchirped Gaussian pulse (pulse width T_0 and power P_0) that propagates linearly through the first dispersive fiber with length L_1 and GVD parameter β_2. Therefore, the envelope in the linear case is given by

$$A_c(z,t)=\sqrt{\frac{P_0T_0}{T(z)}}e^{i\varphi(z,t)}e^{-t^2/T^2(z)} \tag{2}$$

where

$$\begin{aligned}T(z)&=T_0\sqrt{1+(z/L_D)^2},\\ \varphi(z,t)&=\varphi_L(z,t)\quad(z<L_1),\\ \varphi_L(z,t)&=\frac{-(z/L_D)t^2}{2T^2(z)}+\frac{1}{2}\tan^{-1}(z/L_D)\end{aligned} \tag{3}$$

where L_D is the dispersion length and related to GVD parameter by $L_D=|T_0^2\beta_2^{-1}|$, t is time, and z is propagation distance [14]. The model then adds a nonlinear phase term to this solution to include optical nonlinearity. If the nonlinearity is weak enough, the pulse maintains its shape [14] and its envelope is maintains a (dispersed) Gaussian profile with a well-known nonlinear phase that starts to accumulate after the first dispersive fiber

$$\begin{aligned}\varphi(z,t)&=\varphi_L(z,t)+\varphi_{\text{NL}}(z,t)\quad(z>L_1)\\ \varphi_{\text{NL}}(z,t)&=\int_{L_1}^{z}\gamma|A_c(z',t)|^2dz'.\end{aligned} \tag{4}$$

Note that the model includes the linear phase accumulated over both fibers, while the nonlinear phase is only added in the second fiber. This model is based on [16], except that the drop in optical peak power due to dispersion was neglected previously. As opposed to the split-step Fourier method, this analytical model does not take into account the modified dispersion of the nonlinearly-generated frequencies.

A subtle issue in calculating φ_{NL} is that different instants on the optical pulse travel at different speeds, carrying the nonlinear phase with them. The nonlinear phase at any instant along the envelope is then the total nonlinear phase accumulated by that portion of field throughout the fiber. The split-step Fourier method applies the dispersion to the field in the frequency domain as the nonlinear phase is accumulated during propagation, which carries the nonlinear phase with the frequency components automatically; but in the analytical model we must explicitly ensure that the nonlinear phase factor is dispersed along with the pulse envelope. Fortuitously, the dispersion causes each point of the optical pulse to remain the same number of pulse widths from the peak of the pulse as illustrated in Fig. 2. Note that this simplification occurred because we started the nonlinear phase calculation with a chirped Gaussian pulse; arbitrary pulses do not in general satisfy this property. Thus, for each point along the optical pulse, the value in the Gaussian function is constant, and can be taken out of the integral

$$\begin{aligned}\varphi_{\text{NL}}(z,t)&=\gamma P_0e^{-t^2/T^2(z)}\int_{L_1}^{z}\frac{dz'}{\sqrt{1+(z'/L_D)^2}}\\ &=\varphi_{\text{NL}}^{\text{peak}}(z)e^{-t^2/T^2(z)}.\end{aligned} \tag{5}$$

Upon taking the limit of no dispersion ($L_D\to\infty$; equivalent to ignoring the drop in optical power), (5) reproduces the result found in [14], [16], (cf. (4.1.5) and (3.4), respectively):

$$\varphi_{\text{NL}}(z,t)=\gamma P_0(z-L_1)e^{-t^2/T^2(z)}. \tag{6}$$

By substituting the stretch factor $S=(L_1+L_2)/L_1$ (the amount by which the electrical pulse is effectively stretched in time), the nonlinear length $L_{\text{NL}}=(\gamma P_0)^{-1}$, and the dispersion

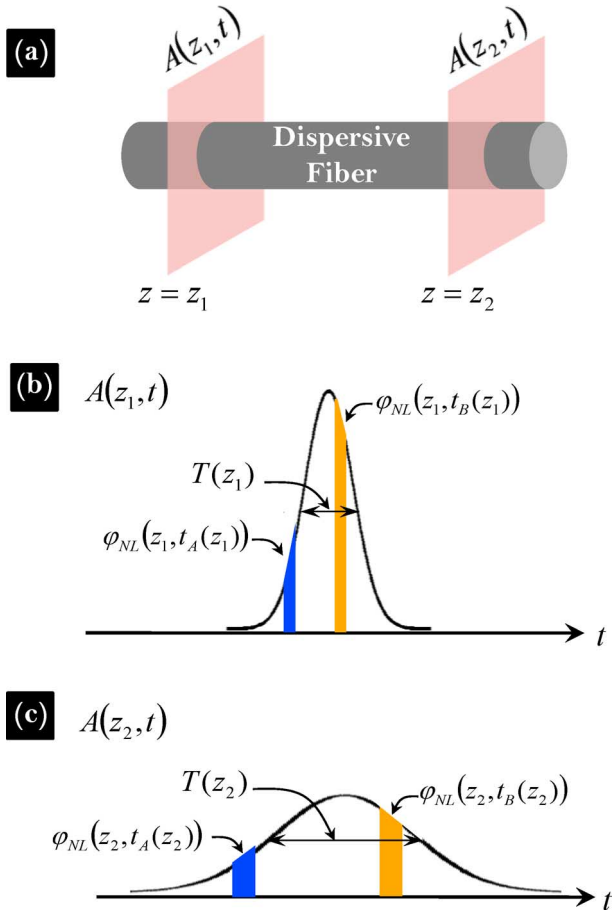

Fig. 2. (a) A section of a typical optical fiber. $A(z_1,t)$ and $A(z_2,t)$ are the slowly varying envelopes of the optical field at distances z_1 and z_2, respectively. (b) Optical field envelope before propagating through a short segment of dispersive fiber. (c) Dispersed optical field envelope after propagating through a short segment of dispersive fiber.

length L_D into (5), the peak nonlinear phase shift (5) after L_1 and L_2 can be obtained

$$\varphi_{\mathrm{NL}}^{\mathrm{peak}} = \left(\frac{L_D}{L_{\mathrm{NL}}}\right)\left(\sinh^{-1}\left(\frac{SL_1}{L_D}\right) - \sinh^{-1}\left(\frac{L_1}{L_D}\right)\right). \tag{7}$$

If $L_1 L_D^{-1} > 2$ and $S > 1$, both of which hold for the TSADC system, then (7) can be very well approximated with a logarithm. In terms of system variables

$$\varphi_{\mathrm{NL}}^{\mathrm{peak}} \approx \left(\frac{L_D}{L_{\mathrm{NL}}}\right)\ln(S) = \frac{\gamma P_1 T_A}{\Delta\lambda |D|}\ln(S), \tag{8}$$

where P_1 is the optical peak power after L_1 and $D = -2\pi c\beta_2\lambda_2^{-2}$ is the GVD parameter in wavelength units. Note that this value is not independent of the fiber lengths, as

$$L_1 = T_A/(\Delta\lambda D);\ L_2 = L_1(S-1). \tag{9}$$

Numerically, this approximation shows an excellent agreement with the split-step Fourier simulations in the absence of RF modulation. The error of the analytical approximation relative to the split-step solution, given by

$$\text{error} = \sqrt{\frac{\int_{-\infty}^{+\infty} |A_{\mathrm{SSFM}}(L_1+L_2,t) - A_c(L_1+L_2,t)|^2 dt}{\int_{-\infty}^{+\infty} |A_{\mathrm{SSFM}}(L_1+L_2,t)|^2 dt}} \tag{10}$$

was found to be less than 0.01% along the entire length of propagation for P_1 up to 300 mW, where A_{SSFM} is the optical envelope as calculated by the split-step Fourier method. If one ignores the nonlinearity in the analytical approximation, the error exceeds 30% even at P_1 of 100 mW. Other analytical approximations, such as the variational method [17] and moment method [14], were compared with the split-step Fourier method as well, but were found to be in worse agreement. This is because in this model we find the time dependence of the nonlinear phase while other methods include the phase through extra parameters (e.g., chirp) in a fixed functional form.

Equation (8) shows that the effect of nonlinearity increases with optical power and stretch factor. Interestingly, the logarithmic term indicates that the nonlinearity does not increase quickly with stretch factor. This can be understood by considering that when the pulse is stretched further, the peak power has decreased and nonlinearity is weaker. In other words, one should safely be able to scale the stretch factor without any excessive optical nonlinearity.

We also briefly note that in each of our simulations the local-error method chose the step size to maintain a constant change of $\varphi_{\mathrm{NL}}^{\mathrm{peak}}$ per step. Intuitively, the error in each step depends on the amount by which the nonlinear and linear operators in the NLSE do not commute, which is dependent on the change in nonlinear phase.

III. Simulations and Results

The TSADC configuration we used to numerically evaluate the performance exploits a prechirped broadband optical pulse (variable optical bandwidth from 5 nm to 32 nm) and modulates the RF signal onto the pulse using a dual-output push-pull Mach–Zehnder modulator. Then the two complementary outputs of the modulator propagate through the dispersive fibers [lossless with dispersion parameter (D) of -100 ps.nm^{-1} km^{-1} and nonlinear coefficient of 5 W^{-1} km^{-1}]. The first dispersive fiber for prechirping and the second dispersive fiber for time-stretching are set to provide a stretch factor of 20, while the total time aperture is kept below 10 ns [see (9)].

The sinusoidal transfer function of the Mach–Zehnder modulator followed by GVD generates the RF signal sidebands and their harmonics. Many techniques have been developed to mitigate and/or cancel out these harmonic distortions [18], [19]. It has been shown that the differential operation utilizing the complementary Mach–Zehnder outputs is able to cancel out the even-order distortions. However, the odd-order distortions cannot be fully eliminated due to the frequency-dependent phase shift caused by GVD. In particular, the 3rd-order distortion limits the performance of the system. The carrier-to-interference ratio in the TSADC is defined as the ratio of the fundamental tone to the 3rd-order harmonic. Fig. 3(a)

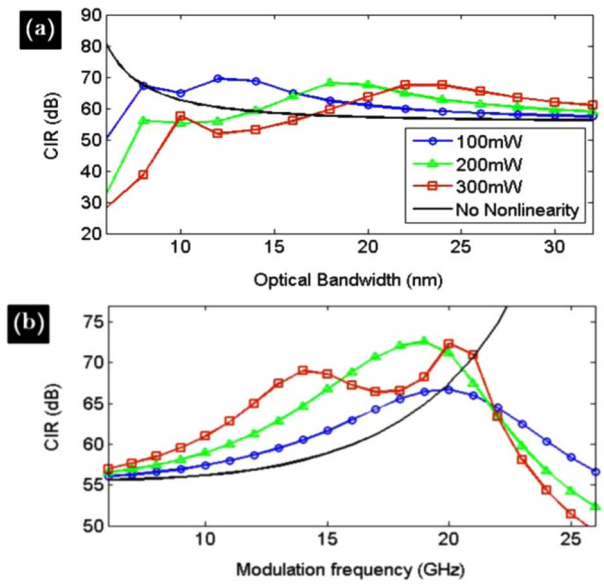

Fig. 3. (a) Carrier-to-interference ratio (CIR) of the TSADC versus optical bandwidth for different optical powers. CIR is defined as the ratio of the amplitude of the fundamental tone to that of the 3rd order harmonic. (b) CIR of the TSADC versus the frequency of the RF signal for different optical powers with constant optical bandwidth (32 nm).

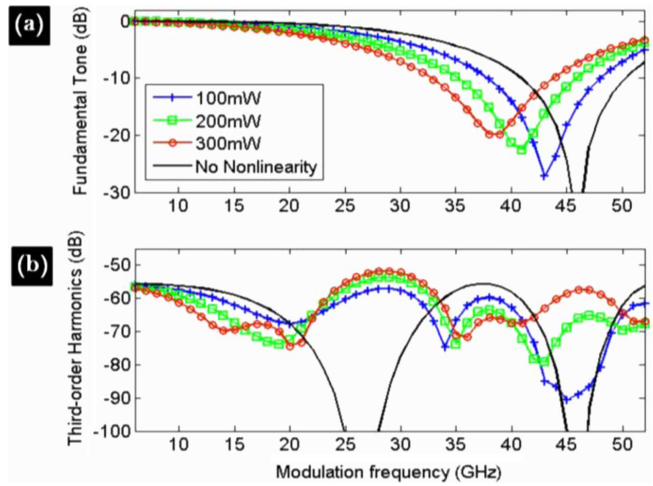

Fig. 4. Single-tone dispersion penalty of the (a) fundamental tone and the (b) 3rd-order harmonic distortion for different optical powers with constant optical bandwidth (32 nm). The dispersion penalty was extracted for a single-tone RF signal sent to the TSADC. The bandwidth limitation imposed by the dispersion penalty becomes more severe at high optical powers.

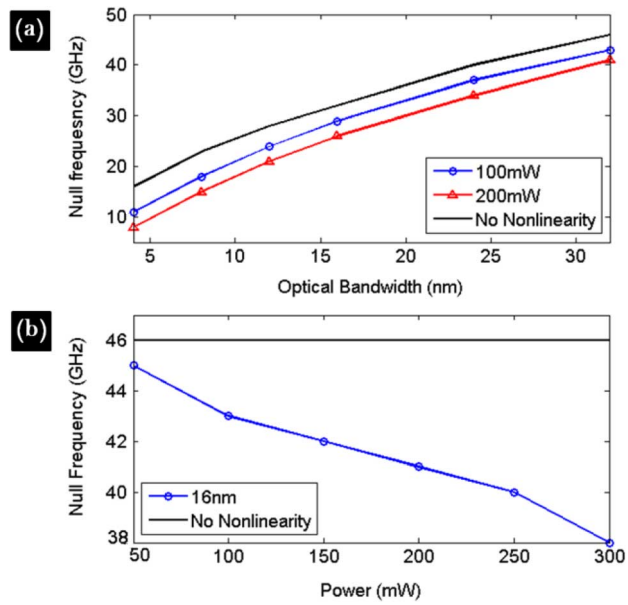

Fig. 5. Single-tone dispersion null frequency versus (a) optical bandwidth for different optical powers and (b) optical power for constant optical bandwidth (16 nm). The null frequency moves higher for larger optical bandwidths and to lower frequencies for higher optical powers.

shows the carrier-to-interference ratio versus optical bandwidth of the source for different optical powers (peak power at the beginning of the second dispersive fiber), while the frequency of the RF signal was constant. At large optical bandwidths, the nonlinear phase shift is small [see also (8)] because the optical pulse disperses faster in the second dispersive fiber. This is manifested in Fig. 3(a) in the convergence of carrier-to-interference ratio for different optical power levels at large optical bandwidths. However, since the optical peak power drops slowly at lower optical bandwidth, the nonlinearity can greatly degrade the carrier-to-interference ratio in the narrowband regime. Fig. 3(b) illustrates the carrier-to-interference ratio versus the frequency of the RF signal for different optical power levels while the optical bandwidth of the optical source is constant (32 nm). The carrier-to-interference ratio improves at low modulation frequencies due to the suppression of the 3rd-order harmonic (see also Fig. 4). However, optical nonlinearity can greatly degrade the carrier-to-interference ratio at high modulation frequencies, limiting the effective number of bits at those frequencies.

The change in carrier-to-interference ratio arises because the RF signal sidebands and their harmonics in the TSADC undergo different linear and nonlinear phase shifts across the RF spectrum and therefore, a fading phenomenon [11], i.e., dispersion penalty, at the photoreceiver output is inevitable. The dispersion penalty for the fundamental tone and 3rd-order harmonic distortion is illustrated in Fig. 4(a)–(b), respectively. The dispersion penalty exists in the linear-optical regime; however, nonlinearity causes a shift in the dispersion-penalty null frequency. This shift can be explained by the analytical approximation developed in the previous section. Since the carrier of the optical pulses is the strongest component, it has the largest influence on the nonlinearity. Therefore, (2) still holds for the carrier even in the presence of RF signal sidebands. The nonlinear phase factor adds with the linear phase in (4) and so shifts the dispersion null in Fig. 4(a). In other words, larger GVD is required for a given RF bandwidth and stretch factor at high optical power levels. Interestingly, we found that if the GVD is anomalous, the dispersion penalty is shifted in the opposite direction; however, use of anomalous GVD fiber is not desirable due to lower dispersion-to-loss ratio and modulation instability.

A set of simulations was performed to understand the behavior of the dispersion null frequency versus optical bandwidth and optical power. As illustrated in Fig. 5(a)–(b), the null frequency goes to higher frequencies for larger optical bandwidths and to lower frequencies for higher optical powers, which is

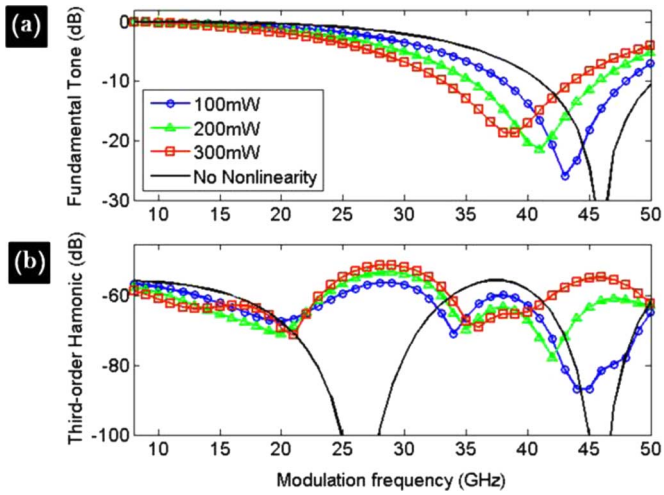

Fig. 6. Two-tone dispersion penalty for the (a) fundamental tone and the (b) 3rd-order harmonic distortion for different optical power levels with constant optical bandwidth (32 nm). The dispersion penalty was extracted for a two-tone RF signal sent to the TSADC. For these plots, the RF tones are chosen so that $f_2 = f_1 + 2$ GHz.

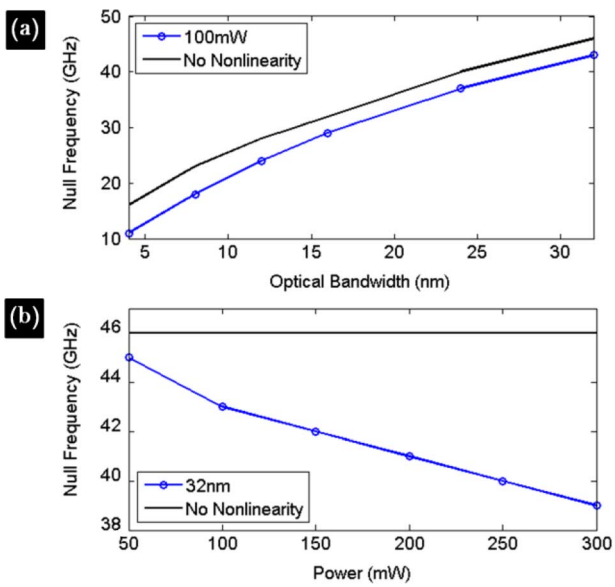

Fig. 7. Two-tone dispersion null frequency versus (a) optical bandwidth for constant optical power (100 mW) and (b) optical power for constant optical bandwidth (32 nm).

due to the dependence of nonlinear phase shift on optical bandwidth and power, as expected from (8). Fig. 6(a)–(b) shows the dispersion penalty when a two-tone (f_1 and f_2) RF signal is sent to the TSADC. Since the intermodulation distortion is minimal, the two-tone dispersion penalty is very similar to the single-tone dispersion penalty. The dependence of dispersion penalty null frequency on optical power and optical bandwidth in the two-tone measurements are illustrated in Fig. 7(a)–(b), respectively. As in the case of the single-tone test, the null frequency goes to higher frequencies for larger optical bandwidths and to lower frequencies for lower optical power levels, which is due to the dependence of the nonlinear phase shift on optical bandwidth and power.

IV. Conclusion

In this paper, we have reported the impact of optical fiber nonlinearity in the photonic time-stretch analog-to-digital converter. We showed that the carrier-to-interference ratio of the time-stretch system is power dependent due to optical nonlinearity. Therefore, the optical nonlinearity limits the maximum effective number of bits that can be achieved at high optical power. It was also shown that the dispersion penalty is power dependent in the presence of optical nonlinearity and can become severe at high optical powers. Furthermore, we have developed an approximate analytical model to qualitatively predict the effect of optical nonlinearity on the carrier of the optical pulse. The results presented here can be generalized to a broad range of optical links.

References

[1] J. Murphy, "Development of high performance analog-to-digital converters for defense applications," in *Proc. Gallium Arsenide Integrated Circuit (GaAs IC) Symp/*, 1997, pp. 83–86.

[2] A. Yen, *Flow Cytometry: Advanced Research and Clinical Applications*. Boca Raton, FL: CRC Press, 1989, vol. 1.

[3] J. da Silva and H. Mendonça, "ADC applications, architectures and terminology," in *Dynamic Characterisation of Analogue-to-Digital Converters*, D. Dallet and J. da Silva, Eds. Dordrecht, The Netherlands: Kluwer, 2005, vol. 860, ch. 1, pp. 3–45.

[4] M. Birk, P. Gerard, R. Curto, L. Nelson, X. Zhou, P. Magill, T. J. Schmidt, C. Malouin, B. Zhang, E. Ibragimov, S. Khatana, M. Glavanovic, R. Lofland, R. Marcoccia, G. Nicholl, M. Nowell, and F. Forghieri, "Field trial of a real-time, single wavelength, coherent 100 Gbit/s PM-QPSK channel upgrade of an installed 1800 km link," in *Proc. OFC/NFOEC*, 2010, pp. 1–3.

[5] L. E. Nelson, S. L. Woodward, S. Foo, X. Zhou, M. D. Feuer, D. Hanson, D. McGhan, H. Sun, M. Moyer, M. O. Sullivan, and P. D. Magill, "Performance of a 46-Gbps dual-polarization QPSK transceiver with real-time coherent equalization over high PMD fiber," *J. Lightw. Technol.*, vol. 27, no. 3, pp. 158–167, Feb. 2009.

[6] P. J. Winzer and R. J. Essiambre, "Advanced optical modulation formats," *Proc. IEEE*, vol. 94, no. 5, pp. 952–985, May 2006.

[7] P. J. Winzer, G. Raybon, H. Song, A. Adamiecki, S. Corteselli, A. H. Gnauck, D. A. Fishman, C. R. Doerr, S. Chandrasekhar, L. L. Buhl, T. J. Xia, G. Wellbrock, W. Lee, B. Basch, T. Kawanishi, K. Higuma, and Y. Painchaud, "100-Gb/s DQPSK transmission: From laboratory experiments to field trials," *J. Lightw. Technol.*, vol. 26, no. 20, pp. 3388–3402, Oct. 2008.

[8] J. Sinsky and P. Winzer, "100-Gb/s optical communications," *IEEE Microwave*, vol. 10, no. 2, pp. 44–57, Apr. 2009.

[9] B. Jalali and F. M. A. Coppinger, "Data Conversion Using Time Manipulation," U.S. Patent 6 288 659, Sep. 11, 2001.

[10] A. S. Bhushan, F. Coppinger, and B. Jalali, "Time-stretched analogue-to-digital conversion," *Electron. Lett.*, vol. 34, pp. 839–841, 2002.

[11] Y. Han and B. Jalali, "Photonic time-stretched analog-to-digital converter: Fundamental concepts and practical considerations," *J. Lightw. Technol.*, vol. 21, p. 3085, Dec. 2003.

[12] S. Gupta and B. Jalali, "Time-warp correction and calibration in photonic time-stretch analog-to-digital converter," *Opt. Lett.*, vol. 33, pp. 2674–2676, 2008.

[13] J. Chou, J. Conway, G. Sefler, G. Valley, and B. Jalali, "150 GS/s real-time oscilloscope using a photonic front end," in *Proc. MWP/APMP*, 2008, pp. 35–38.

[14] G. P. Agrawal, *Nonlinear Fiber Optics*, 4th ed. Burlington, MA: Academic Press, 2007.

[15] O. V. Sinkin, R. Holzlöhner, J. Zweck, and C. R. Menyuk, "Optimization of the split-step fourier method in modeling optical-fiber communications systems," *J. Lightw. Technol.*, vol. 21, no. 1, p. 61, Jan. 2003.

[16] M. J. Potasek, G. P. Agrawal, and S. C. Pinault, "Analytic and numerical study of pulse broadening in nonlinear dispersive optical fibers," *J. Opt. Soc. Amer. B*, vol. 3, pp. 205–211, Feb. 1986.

[17] D. Anderson, "Variational approach to nonlinear pulse propagation in optical fibers," *Phys. Rev. A*, vol. 27, pp. 3135–3145, Jun. 1983.

[18] S. Gupta, B. Jalali, J. Stigwall, and S. Gait, "Demonstration of distortion suppression in photonic time-stretch ADC using back propagation method," in *Proc. IEEE Int. Topical Meeting Microw. Photon.*, 2007, pp. 141–144.
[19] S. Gupta, G. C. Valley, and B. Jalali, "Distortion cancellation in time-stretch analog-to-digital converter," *J. Lightw. Technol.*, vol. 25, pp. 3716–3721, Dec. 2007.

Ali M Fard (M'08) received the B.Sc. degree in electrical engineering from the University of Tehran, Tehran, Iran, in 2007 and the M.Sc. degree in electrical engineering from the University of California Los Angeles in 2009, where he is currently pursuing the Ph.D. degree in electrical engineering, physical and wave electronics.

He has been working as Research Assistant in the Photonics Laboratory, University of California Los Angeles since 2007. His research interests include microwave photonics and biophotonics for biomedical and defense applications. He has published over 25 journal and conference papers. He is also a co-inventor of 3 pending patents.

Mr. Fard is a member of the Optical Society of America (OSA) and SPIE. He is also the founding president of UCLA OSA Student Chapter, and the founding vice-president of UCLA SPIE Student Chapter.

Peter T.S. DeVore received the B.A. degree in physics from the University of California Berkeley in 2008 and the M.S. degree in physics from the University of California Los Angeles in 2010, where he is working toward the Ph.D. degree in physics in the Photonics Laboratory.

He has been working as research assistant in the Photonics Laboratory at UCLA since 2008. His research interests include microwave photonics and applications of optofluidics to biophotonics.

Mr. DeVore is a student member of OSA and SPIE, and is a founding officer of the OSA Student Chapter at UCLA and the SPIE Student Chapter at UCLA.

Daniel R. Solli received the Ph.D. degree in physics from the University of California, Berkeley.

He went to the University of California, Los Angeles (UCLA) for a postdoctoral position where he received the UCLA Chancellor's Award for Postdoctoral Research. He currently works with UCLA and the University of Göttingen, Germany. He enjoys interdisciplinary research topics and his present interests include ultrafast measurements, real-time spectroscopy, optical rogue waves and nonlinear phenomena, silicon photonics, and various topics in chemistry. His journal publications have received over 500 total citations.

Bahram Jalali (F'04) is the Northrop-Grumman Optoelectronics Chair Professor of Electrical Engineering, University of California, Los Angeles (UCLA) with joint appointments in the California NanoSystems Institute (CNSI) and the UCLA School of Medicine. He received the Ph.D. in applied physics at Columbia University, New York, in 1989.

He was with Bell Laboratories in Murray Hill, New Jersey until 2002 before coming to UCLA. He serves on the Board of Trustees of the California Science Center, and the Columbia University School of Engineering and Applied Sciences. He has published over 350 journal and conference papers, and holds 9 patents.

Dr. Jalali is a Fellow of the Optical Society of America (OSA), and the American Physical Society (APS). He is the recipient of the R.W. Wood Prize from Optical Society of America for the invention and demonstration of the first Silicon Laser. In 2005 he was elected into the Scientific American Top 50, and received the BrideGate 20 Award in 2001 for his entrepreneurial accomplishments.